A Model-Based Investigation of Manipulator Characteristics and Pilot/Vehicle Performance

Ronald A. Hess*
NASA Ames Research Center, Moffett Field, California

A structural model of the human pilot has been introduced recently and discussed in the literature. The model has been used to provide a rationale for certain nonlinear pilot control behavior such as stick pulsing and has served as a framework for studying aspects of motor skill development. In light of the theoretical background provided by the model, the dependence of pilot equalization capabilities on manipulator characteristics is discussed. In addition, some recent phenomena associated with pilot/vehicle performance in glide slope tracking in short takeoff and landing aircraft are reviewed. The apparent contribution of the cockpit manipulator (throttle) characteristics to these phenomena is outlined.

Introduction

ACTIVE manual control of any physical system typically involves the use of a manipulator as the primary interface between the human and the system being controlled. Control sticks and rudder pedals in aircraft, and steering wheels and accelerator pedals in automobiles, are obvious examples. Studies such as those by Herzog[1] and Merhav and Ya'Acov[2] have capitalized upon the man-manipulator interface to improve performance in certain tracking tasks. In pilot modeling, the dynamics of the manipulator, if important in the frequency range of interest for manual control (typically $0.1 \leq \omega \leq 10$/s), are usually considered a part of the dynamics of the controlled element. Proprioceptive feedback from the manipulator traditionally has not been assumed to be a major factor in the pilot's equalization capabilities, although its contribution to the operation of the particular neuromuscular system controlling the manipulator has been recognized as extremely important.[3,4]

Recently, the author[5-8] has introduced and discussed what has been called a structural model of the human pilot in which proprioceptive feedback plays a *fundamental* role in determining pilot equalization characteristics. Because of this feedback structure, this model may offer more insight into the effects of certain manipulator characteristics upon pilot equalization than would other modeling approaches. In the next section, this model will be discussed briefly and some implications of the model structure regarding manipulator characteristics will be outlined. With the model serving as a theoretical framework some specific empirical examples of manipulator effects involving glide slope tracking in STOL aircraft will be discussed.

Structural Mode and Manipulator Characteristics

The structural model of the human pilot proposed by the author has been discussed at some length in the literature[5-8] and hence will only be outlined here. Figure 1 is a block diagram of this model for compensatory tracking behavior. The model in Fig. 1 has been divided into "central nervous system" and "neuromuscular system" components, a division intended to emphasize the nature of the signal-processing activity involved. System error $e(t)$ is presented to the pilot via a display with dynamics Y_{de}. The rate of change of the displayed error is assumed to be derived from $e_d(t)$. The process of deriving error rate is assumed to entail a computational time delay of τ_l s. Constant gains K_e and $K_{\dot{e}}$ multiply the signals $e_d(t)$ and $\dot{e}_d(t-\tau_l)$, respectively. The switch allows either of these two signals to be used as driving signals to the remainder of the model. A discussion regarding the utility of error rate control is provided in Ref. 8. The action of the switch is parameterized by the variable P_l, which represents the probability that the switch will be in position 1 (error-rate control) at any instant in time. A central time delay of τ_0 s is included to account for the effects of latencies in the visual process sensing $e_d(t)$, motor nerve conducting times, etc. The resulting signal, $u_c(t)$, provides a command to a closed-loop system, which consists of a model of the open-loop neuromuscular dynamics of the particular limb driving the manipulator, Y_{pn}. Other system components include elements Y_f and Y_m, which emulate, at least approximately, the combined effects of the muscle spindles, Golgi tendon organs, and the dynamics associated with higher level signal processing. The form of Y_m is determined by the order of the controlled-element dynamics $Y_c(j\omega)$ in the region of open-loop crossover. The order is given by the integer k which is obtained by representing $Y(j\omega)$ as

$$Y_c(j\omega)\Big|_{\omega=\omega_c} = \frac{K}{(j\omega)^k} \tag{1}$$

where ω_c represents the pilot/vehicle crossover frequency; i.e., that value of ω for which $|Y_p Y_c(j\omega)| = 1.0$. A colored noise $n_u(t)$ is injected at the pilot's output as remnant. As pointed out in Ref. 7, the signal $u_m(t)$ is really proportional to the time rate of change of vehicle output due to control activity, and as such, is a form of rate feedback.

We will now briefly review some past results in which the structural model was utilized to match experimentally-derived pilot describing functions with controlled-element dynamics of K, K/s, and K/s^2. As will be seen, each of these dynamics makes specific demands upon the feedback structure of the model (and presumably upon the human), which, in turn, will be related to manipulator characteristics.

The first three rows of Table 1 show model parameters selected to give describing-function matches for systems with controlled-element dynamics of K, K/s, and K/s^2. Table 2 shows the variation in pilot dynamics with increases in the order of the controlled-element dynamics. The second column of Table 2 gives the simplest representation of pilot input-output characteristics in terms of leads, lags, and time delays.[4] It should be noted that τ_e varies with the order of the

Submitted Oct. 30, 1981; revision received Jan. 3, 1983. This paper is declared a work of the U.S. Government and therefore is in the public domain.

*Research Scientist. Presently, Associate Professor, Department of Mechanical Engineering, University of California, Davis, Calif. Member AIAA.

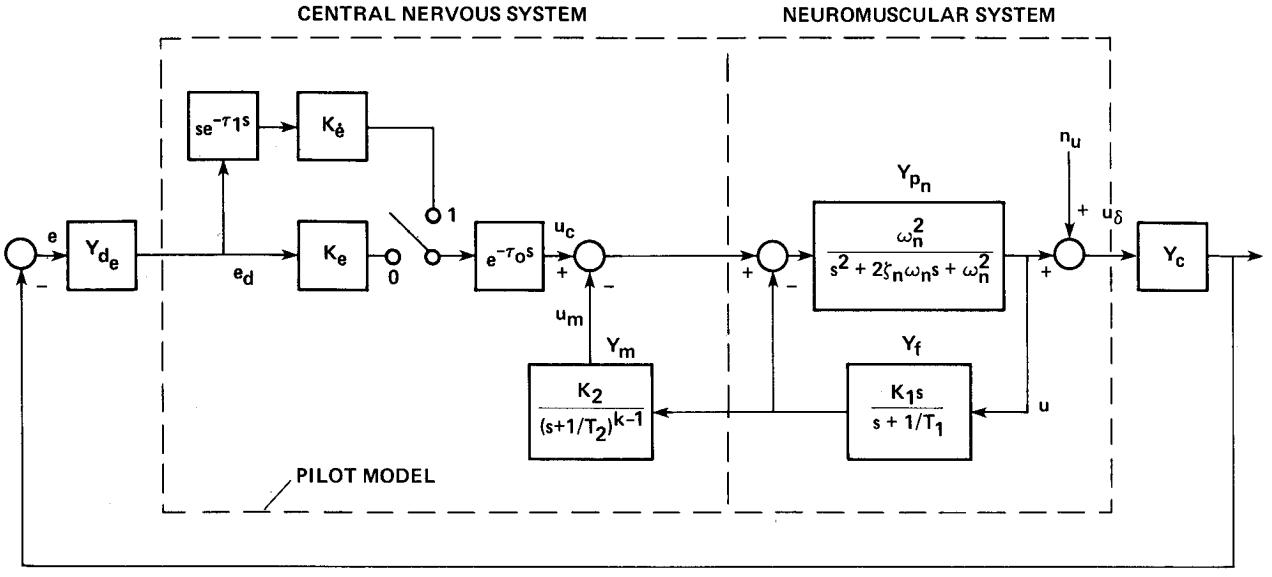

Fig. 1 The structural model of the human pilot.

Table 1 Structural model parameter values

Controlled-element dynamics, Y_c	Model parameters											
	k	K_e	$K_{\dot{e}}$	K_2	P_1	T_1	T_2	K_1	τ_0	τ_1	ζ_n	ω_n
K	0	11.1	2.13	2.0	0.05	5.0	5.0	1.0	0.14	0.2	0.707	10.0
K/s	1	22.2	3.42	2.0	0.05	5.0	–	1.0	0.14	0.2	0.707	10.0
K/s^2	2	26.2	10.50	10.0	0.20	2.5	2.5	1.0	0.14	0.2	0.707	10.0
$(d/\delta_T)'$	0[a]	0.0	87.50	50.0	1.00	2.0	0.5	1.0	0.20	0.0	0.707	10.0
δ_{TFD}/δ_T	0[a]	0.0	87.50	50.0	1.00	2.0	0.5	1.0	0.50	0.2	0.707	10.0
δ_{TFD}/δ_T	1	0.77	0.0	10.0	0.00	0.2	–	1.0	0.50	–	0.707	10.0

[a] Internal model appropriate for rate tracking.

Table 2 The adaptive pilot

Controlled element Y_c	k	Simplified pilot dynamics, Y_p	Required proprioceptive feedback
K	0	$K_p e^{-\tau_e s}/(T_l s+1)$	$du_\delta(t)/dt$
K/s	1	$K_p e^{-\tau_e s}$	$u_\delta(t)$
K/s^2	2	$K_p(T_L s+1)e^{-\tau_e s}$	$\int u_\delta(t)dt$

controlled element.[4] The author has indicated that this variation in effective time delay can be explained by changes in the inner-loop dynamics of the structural model which occur as a consequence of the human's adapting to different controlled-element dynamics.[7]

It is now useful to examine the type of inner-loop dynamics which are hypothesized to exist for each of the three controlled-element types and show how the third column of Table 2 is obtained. The third column shows the simplified form of the proprioceptive feedback implied by the combination of $Y_f Y_m$ in Fig. 1. For example, for $Y_c = K/s$, $k=1$, and from Fig. 1

$$Y_f Y_m = K_1 K_2 s/(s+1/T_1) \tag{2}$$

If $1/T_1$ is significantly less than ω_c, $Y_f Y_m$ looks very much like a pure gain in the important region of open-loop crossover. Thus, row 2, column 3 of Table 2 shows that the required proprioceptive feedback for controlling K/s dynamics is applied force or displacement $u_\delta(t)$. This force or displacement is defined relative to a set point or regulation point; e.g., the equilibrium position of a spring-restrained control stick. K/s dynamics have long been associated with the most desirable "effective-vehicle" characteristics for single-axis systems under manual control.[9] Here, "effective vehicle" refers to the sum total of the dynamics in series with the pilot, i.e., dynamics associated with displays, control systems, and the vehicle itself. In terms of the classical servomodel of the human pilot (likened to column 2 of Table 2), a "pure-gain" pilot model results with K/s dynamics, i.e., no pilot equalization is required. In terms of the structural model, which inherently contains two feedback loops, only feedback of proprioceptively sensed force or displacement is needed. The same cannot be said for $Y_c = K/s^2$; here $k=2$, and, from Fig. 1,

$$Y_f Y_m = K_1 K_2 s/(s+1/T_1)(s+1/T_2) \tag{3}$$

If $1/T_1$ and $1/T_2$ are significantly less than ω_c, $Y_f Y_m$ looks very much like an integrator in the important region of crossover. Thus, row 3, column 3, of Table 2 shows that the required proprioceptive feedback for controlling K/s^2 dynamics is the integral of applied force displacement from some set point or regulation point. A rationale for human operator pulsive control behavior was offered in Ref. 6 based upon the hypothesis that humans attempt to reduce the computational burden of time integration of $u_\delta(t)$ in higher levels of the central nervous system. Lastly, consider $Y_c = K$, $k=0$, and, from Fig. 1,

$$Y_f Y_m = K_1 K_2 (s+1/T_2)/(s+1/T_1) \tag{4}$$

If $T_1 \doteq T_2$, or $1/T_1$ and $1/T_2$ are significantly less than ω_c, $Y_f Y_m$ takes the form of a differentiator in the region of crossover. Thus, row 1, column 3, of Table 2 shows that the

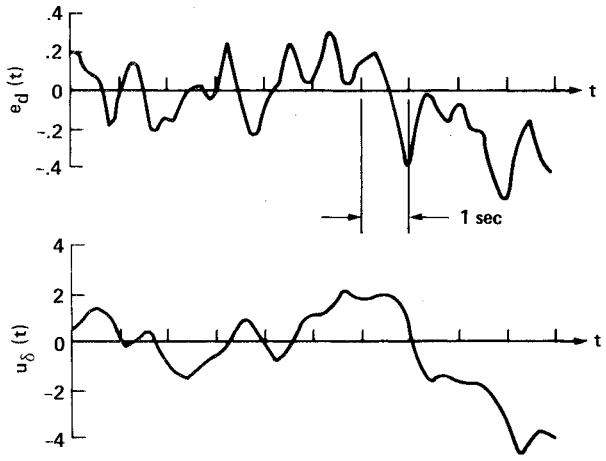

Fig. 2 Error and control from structural model, K controlled-element dynamics.[6]

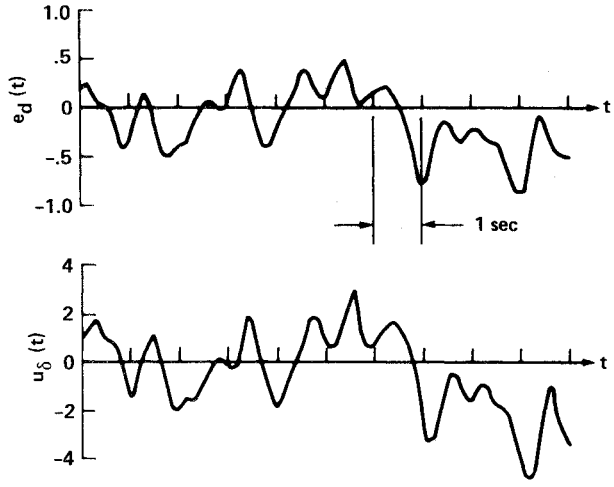

Fig. 3 Error and control from structural model, K/s controlled-element dynamics.[6]

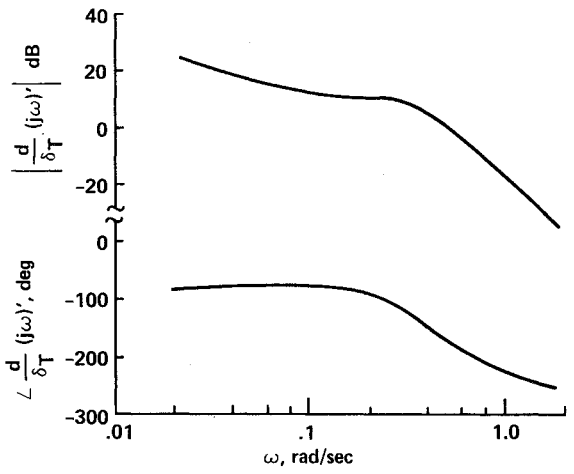

Fig. 4 Vertical flight path to throttle characteristics for configuration AP1.[13]

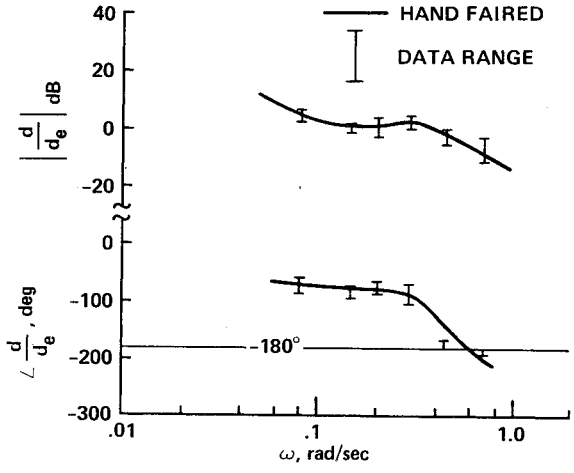

Fig. 5 Measured pilot/vehicle transfer function for configuration AP1.[13]

required proprioceptive feedback for controlling K dynamics is the time derivative of $u_\delta(t)$. Again, assuming the validity of the model of Fig. 1, this differentiation might also be accompanied by considerable activity in the higher levels of the central nervous system. However, two things may mollify this situation. First, as Fig. 1 and Table 2 indicate, the pilot dynamics u_δ/e_d for this controlled element contain a first-order lag. This inherent filtering action of the error signal makes the pilot output $u_\delta(t)$ rather smooth and low frequency in nature. This is exemplified in Figs. 2 and 3 taken from Ref. 6 where the structural model was digitally simulated as part of a single-axis tracking task. Figure 2 shows segments of $e_d(t)$ and $u_\delta(t)$ for $Y_c=K$, whereas Fig. 3 shows the same variables for $Y_c=K/s$. Notice the lower frequency content of $u_\delta(t)$ in Fig. 2 as opposed to that in Fig. 3. Second, the muscle spindles and Golgi tendon organs themselves can provide direct rate information.[10] This means that differentiation, as an operation in the higher levels of the central nervous system, may be obviated. In summary, then, the model suggests that lack of manipulator set point information should not be a handicap when the controlled-element dynamics take on the form of pure gain in the region of crossover. This is an important point and will enter into the discussion of the STOL aircraft glide slope tracking problem in the next section.

In each of Eqs. (2-4), the selection of T_l must, if only in an approximate sense, take into account the limitations of the proprioceptors in the limb effecting control. As a pertinent example, it is not likely in the case of Eq. (2) that $Y_f Y_m$ can be made to exhibit pure gain characteristics around crossover if 1) ω_c is quite low (0.1-0.5 rad/s), *and,* 2) a manipulator is being used which does not provide adequate low-frequency set point information. In other words, it is unlikely that adequate low-frequency proprioceptive information *relative to a set point* can be obtained by the spindles or tendon organs when manipulators are used with no centering characteristics. The joint-angle sensors can provide relatively precise information about relative limb positions, but this is not necessarily synonymous with precise information about manipulator set point. This is particularly true when the manipulator motion utilized in tracking involves angular limb rotation, which is a small percentage of the maximum rotation possible. As a pertinent example, the maximum throttle lever rotation in one of the STOL aircraft experiments to be studied here was only about ±7 deg from the set point.

To the author's knowledge, there has been no systematic study of manipulator effects when the first of the aforementioned criteria was met, i.e., low ω_c. For example, the work of McRuer and Magdaleno[11] and Gordon-Smith[12] involved crossover frequencies of 2 rad/s and above. Thus, the inclusion of only two empirical examples in the next section was due to the relative paucity of data for tracking situations characterized by low-frequency manipulator motion.

Empirical Examples of Manipulator Effects

For the purpose of exposition, we will now review a pair of experimental studies primarily involving the flight path

control of STOL vehicles. The first involves a simulation study, while the second encompasses simulation and flight test. These experiments are pertinent to this discussion since, in each case, certain aspects of pilot/vehicle dynamics and performance will be related to manipulator characteristics via the structural model just discussed.

Case 1

Reference 13 describes an investigation of various vehicle dynamics using a piloted simulation of a powered-lift STOL aircraft during landing approach. For the configurations evaluated, vertical flight path control was accomplished almost exclusively by throttle. In addition, very little column activity was needed for attitude/airspeed control. This was not accidental, since an attitude-hold stability augmentation system (SAS) was designed and utilized for the express purpose of minimizing pilot activity with the longitudinal control column.

Figure 4 and Table 3 show the dynamics of one of the configurations analyzed. The pertinent transfer function is

$$(d/\delta_T)' = (N^{\dot{d}}_{\delta_T})'/s\Delta' \qquad (5)$$

where d represents vehicle glide slope deviations and δ_T is throttle movement. The prime is meant to emphasize the fact that an inner attitude loop is being closed by the SAS. No inner-loop attitude closure by the pilot is included, an assumption proved valid in simulation. Table 3 lists the pertinent vehicle dynamics. It is imperative to point out that engine rpm was controlled by overhead throttles with no centering characteristics, which provided no arm support that might aid in determining set point position.

Figure 5 shows the pilot/vehicle transfer function for the configuration of Fig. 4 measured at six frequencies around crossover. The solid line is hand-faired through the data. The pilot/vehicle transfer functions were measured using a Fourier transform technique with "pseudoturbulence" represented by a sum of sinusoids. This turbulence was implemented by providing a "command" glide slope signal d_c on the glide slope deviation indicator. Thus, d represents vehicle output relative to some trim value and $d_e = d_c - d$. The open-loop transfer function of Fig. 5 is of interest for four reasons: First, the crossover frequency appears to be somewhere between 0.3 and 0.4 rad/s; a relatively low value for manual control experiments. Second, the pilot is not particularly successful in forcing the open-loop pilot/vehicle characteristics into a K/s-like form in the region of crossover. Third, the low-frequency phase data exhibits none of the "phase droop" normally associated with such pilot/vehicle open-loop transfer function measurements. Finally, fitting this data with a simple lead-lag model would require an effective time delay of 0.8 s; quite a large value for manual control experiments. It should also be noted that the vehicle dynamics of configuration AP1 were rated as only marginally acceptable to the pilots (Cooper-Harper pilot ratings of 4-7).

We will now show that these four characteristics can be produced by the structural model of Fig. 1. Figure 6 shows the model-generated pilot/vehicle transfer function. The model parameters are listed in the fourth row of Table 1. Note that the low-frequency portion of Y_f is providing the required rate information (du_δ/dt). The model fit was obtained by assuming that the pilot was controlling rate alone. This assumption was necessary to achieve an acceptable fit to the data. Actually, the error-rate loop would serve as an inner loop to an outer, error-loop closure. However, the fact that a reasonable fit to the data could be obtained by considering error-rate control alone suggests that this control dominates. This is corroborated by experimental results from Ref. 13 in which it was stated, "all of the pilots indicated that the technique for glide slope was primarily to control glide slope deviation rate ($\dot{d}$)."

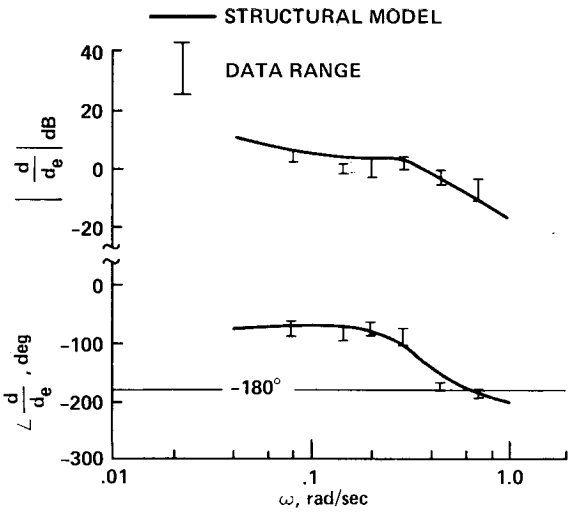

Fig. 6 Comparison of experimental and model-generated transfer functions for configuration AP1.

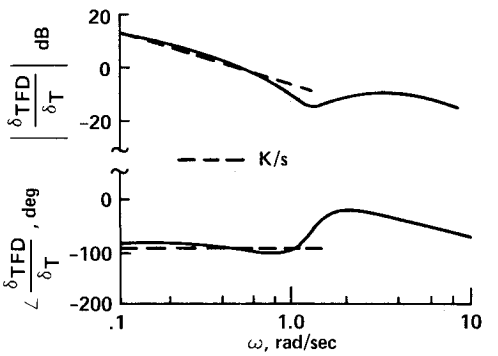

Fig. 7 Effective vehicle (director plus aircraft) for throttle control.[14]

Table 3 STOL configuration AP1[13]

Trim airspeed, knots	75.0
Flight path angle, deg	−6.0
Trim pitch attitude, deg	1.87
Trim power setting, %	30.6

$$\Delta' = (s+0.25)(s+0.36)(s+0.67)(s+8.32)[s^2+2(0.5)(0.33)s+0.33^2]$$

$$(N^{\dot{d}}_{\delta_T})' = 0.167(s+0.475)(s+1.75)(s+8.3)[s^2+2(0.99)(0.163)s+0.163^2]$$

Prime indicates inner attitude loop closed by SAS.

Using the structural model, we can now provide a rationale for this rate-tracking activity. The transfer function $(\dot{d}/\delta_T)'$ will exhibit characteristics much like pure gain for $\omega \leq 0.3$ rad/s. Such characteristics have been hypothesized here to be quite acceptable for manipulators which do not provide adequate set point information, such as the engine throttles used in Ref. 13. Normally, exclusive rate control would carry a workload burden imposed by the necessity of deriving rate information from displacement information. However, in the simulation of Ref. 13, rate information was available directly from the instantaneous vertical speed indicator (IVSI) in the cockpit. Again, quoting from Ref. 13, the actual piloting technique was

"a) Keep $\dot{d}$ at a very low level by controlling IVSI with power, e.g., find a target IVSI that keeps the glide slope bug stationary on the display (nominally 800 ft/min).

"b) If glide slope error (d) is diverging, try to first zero $\dot{d}$, then adjust power so d is slowly converging (i.e., pick a new target sink rate on the IVSI).

"c) If the glide slope error is less than one dot, make very small power adjustments (if any)."

Since rate information was available directly, and, as the quote above indicates, was used extensively by the pilots, the delay normally associated with rate information in the structural model, τ_1, was set to zero. To account for scanning delays, τ_0 was increased from the nominal 0.14 s to 0.2 s. Note that the model captures the salient features of the data including the four "anomalies" mentioned previously. In particular, note that no large time delays have to be hypothesized to match the phase lag data. It also appears that all of these anomalies have their origin in the characteristics of the manipulator and in the availability of explicit rate information.

Case 2

Next, let us consider the results of an investigation reported in Ref. 14. In this study, a flight test program was carried out to assess the feasibility of piloted instrument approaches along predefined, steep, curved, and decelerating approach profiles in powered-lift aircraft operating on the backside of the power-required curve. Separate stability augmentation systems for attitude and speed were provided, as well as a supporting flight director and special electronic cockpit displays. Of particular interest was a problem encountered in glide slope tracking using a throttle flight director which utilized K/s-like effective-vehicle characteristics in the frequency range $0.1 \leq \omega \leq 1.0$ rad/s. Figure 7 shows the effective-vehicle characteristics (director plus aircraft). Although the K/s dynamics do not extend beyond 1.0 rad/s, no additional and deleterious phase lags accrue beyond this region. Figure 8 shows undesirable oscillatory glide slope tracking characteristics revealed in flight tests for this configuration.

The question now arises regarding the pilot's control strategy for this effective vehicle. Two obvious possibilities are: 1) rate control predominates as in the previous example,

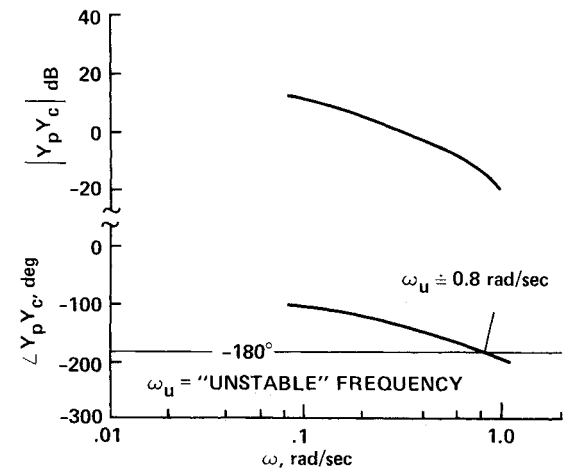

Fig. 10 Model-generated transfer function indicating probable pilot dynamics for displacement control of effective vehicle of Fig. 7.

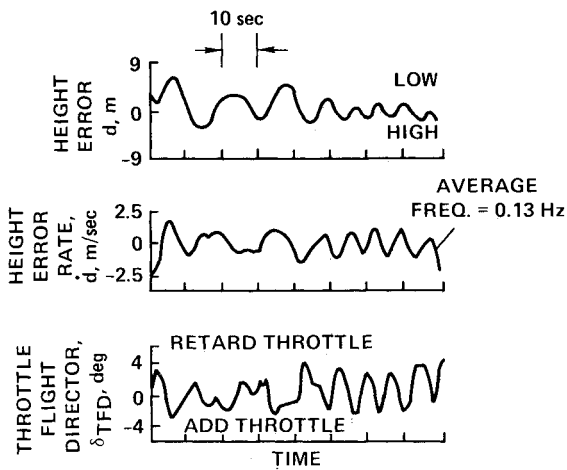

Fig. 8 Glide slope tracking characteristics of aircraft.[14]

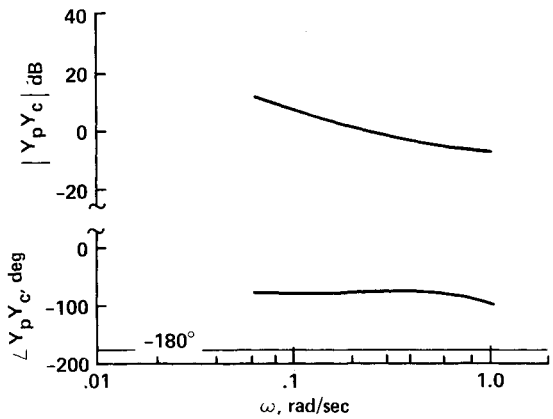

Fig. 9 Model-generated transfer function indicating probable pilot dynamics for rate control of effective vehicle of Fig. 7.

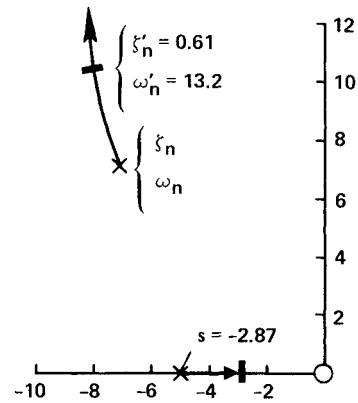

Fig. 11 Root locus diagram for structural model inner-loop closure, model characteristics shown in Fig. 10.

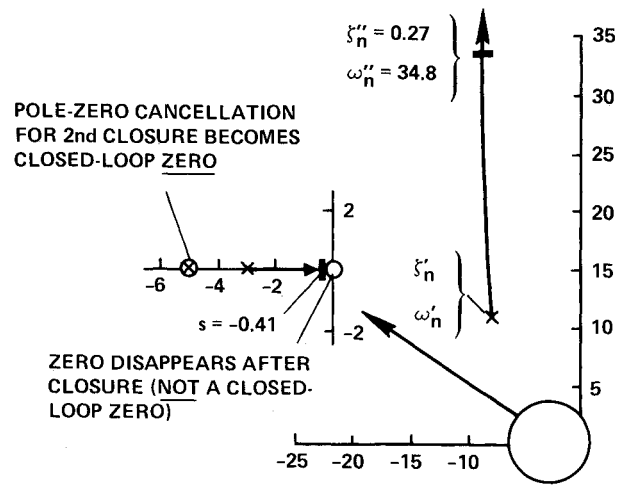

Fig. 12 Root locus diagram for structural model outer-loop closure, model characteristics shown in Fig. 10.

or 2) displacement control predominates. In the first case, the pilot's internal model of the effective vehicle in the frequency range $\omega \leq 1.0$ rad/s would be a pure gain ($k=0$). According to the structural model, this would allow the manipulator to be suited to the dynamics. However, unlike the simulation just studied, rate information in the form of $\dot{\delta}_{TFD}$ (rate of change of throttle director signal) is not explicitly available and would have to be derived by the pilot. Probable pilot/vehicle dynamics for this case are shown in Fig. 9. The structural model parameters are shown in the fifth row of Table 1. With the exception of τ_0 and τ_1, they are identical to the parameters which yielded the match of Fig. 9 (fourth row of Table 1).

The value of τ_0 was increased from 0.2 to 0.5 s to account for the likelihood of considerably more scanning activity occurring in the study of Ref. 14 (a flight test) than in that of Ref. 13 (a simulation). The value of τ_1 was increased from 0 to 0.2 s to account for the fact that rate information had to be derived. As Fig. 9 indicates, stability margins are more than adequate. However, the necessity of continuously deriving rate information from the displayed flight director signal δ_{TFD} may lead to high workload and inadequate time to control the remaining two flight directors and scan the status displays in the cockpit. In addition, from the pilot's viewpoint, rate control alone may not yield acceptable performance.

Consider, on the other hand, the more probable situation in which the pilot controls displacement. Here, the pilot's internal model of the effective vehicle in the frequency range $\omega \leq 1.0$ rad/s would be K/s ($k=1$). According to the structural model, the manipulator characteristics are not well suited to those of the effective vehicle, since again, low crossover frequencies are implied and engine rpm was controlled by overhead throttles with no centering characteristics. Figure 10 shows the probable pilot/vehicle dynamics for this case under this assumption. The model parameters are given in the sixth row of Table 1. For the sake of simplicity, no switching is assumed to occur, i.e., $P_1=0$. The most significant differences are the values of T_1 and τ_0. The rationale behind the revised value of τ_0 has been given. As opposed to the previous two models, the hypothesized lack of adequate manipulator position information (u_δ) must now be included in the model. The decreased value of T_1 is intended to account for this. This reduction means that the "break frequency" of the washout element Y_f of Fig. 1 is moved to higher frequencies, thus reducing the amount of low-frequency information available. Indeed, with $T_1=0.2$ s only du_δ/dt is available for $\omega \leq 5.0$ rad/s.

The effect of this change is rather dramatic as can be seen by comparing the phase angle plots of Figs. 9 and 10. This lag increment is obviously not due to any changes in the delay τ_0. Rather, the closure of the two inner loops of the model causes a real root to migrate to a position $s=-0.4$. This is demonstrated in the two root locus diagrams for those closures shown in Figs. 11 and 12. Note from Fig. 10 that a closed-loop instability is possible at $\omega=0.8$ rad/s (0.13 cycles/s). This is seen to compare very favorably with the frequency of the path rate oscillations evident in Fig. 8, where five cycles occur in approximately 38 s. These oscillations constitute the glide slope tracking problem alluded to briefly at the beginning of our discussion of the experiments of Ref. 14. Although the oscillations of Fig. 8 represent a worst-case example, they typified the glide slope tracking characteristics of the pilot/vehicle system and were experienced to some degree by all of the evaluation pilots. The model results should not be interpreted as a prediction, but rather as a rationale for the existence of a low-frequency oscillation in the glide slope tracking for this effective vehicle/manipulator combination. Note that in order to produce an unstable frequency at 0.8 rad/s using a crossover model of the pilot,[7] an effective time delay on the order of 1.5 s would have to be hypothesized!

From what has been discussed thus far, a solution to the flight path oscillation problem would appear to lie in changing the characteristics of either the throttle or the effective vehicle. The latter course was chosen in Ref. 14 and the dynamics of the effective vehicle (director plus aircraft) were changed from K/s to K. This was accomplished by incorporating a glide slope tracking law based on angular beam deviation (effectively $\dot{d}$), and feeding back washed-out throttle position to extend the system bandwidth. The reader is referred to Ref. 14 for details. Figure 13 shows the modified effective-vehicle dynamics. The rolloff at frequencies beyond 5 rad/s is due to a first-order filter being implemented to smooth the director signal at high frequencies. Figure 14 shows the resulting flight test results with the modified director (note the change in scales in the ordinates between Figs. 8 and 14 taken directly from Ref. 14). Performance is improved rather dramatically. Quoting from Ref. 14:

"During the limited flight evaluation of these alternative throttle flight-director control laws, and during the course of gathering the simulator data, pilot commentary indicated very little tendency towards oscillatory glidepath tracking characteristics.... Once a correction was made, attention could temporarily be diverted to other display-scanning tasks without large errors developing in the throttle director bar."

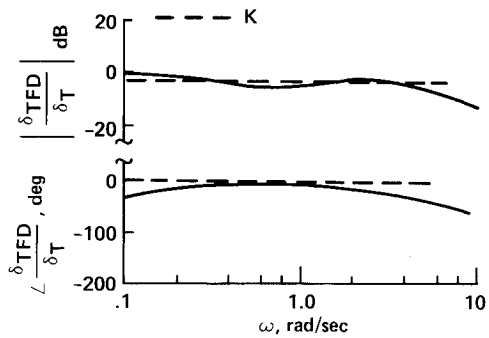

Fig. 13 Modified effective vehicle (director plus aircraft) for throttle control.[14]

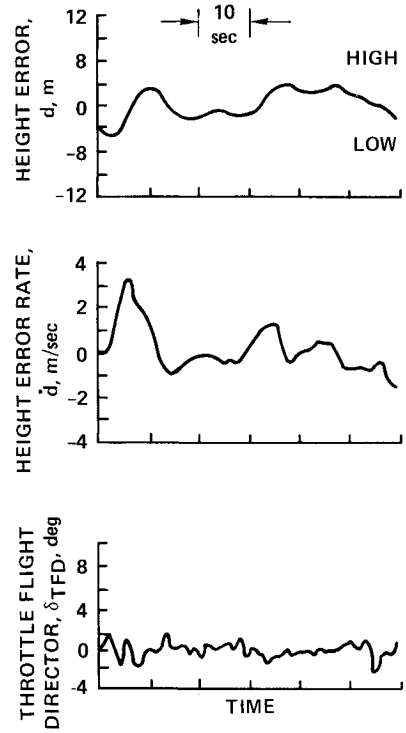

Fig. 14 Glide slope tracking characteristics of aircraft with modified flight director.[14]

Concluding Remarks

The research discussed herein was intended to point out that ideal effective-vehicle dynamics for manual-control problems can be dependent upon manipulator characteristics. A structural model of the human pilot which incorporated explicit proprioceptive feedback was used as a framework for interpreting some simulation and flight test results. The model was able to match measured pilot transfer function data exhibiting "anomalous" characteristics and was able to provide a rationale for oscillatory pilot/vehicle behavior. In the latter case, the model verifies what was found to be a successful approach for improving the glide slope tracking performance of the aircraft and flight director system exhibiting the oscillatory characteristics.

References

[1]Herzog, J.H., "Proprioceptive Cues and Their Influence on Operator Performance in Manual Control," NASA CR-1248, 1969.

[2]Merhav, I.J. and Ya'Acov, O.B., "Control Augmentation and Work-Load Reduction by Kinesthetic Information from the Manipulator," *IEEE Transactions on Systems, Man, and Cybernetics,* Vol. SMC-6, Dec. 1976, pp. 825-835.

[3]Magdaleno, R.E. and McRuer, D.T., "Experimental Validation and Analytical Elaboration for Models of the Pilot's Neuromuscular Subsystem in Tracking Tasks," NASA CR-1757, 1971.

[4]McRuer, D.T. and Krendel, E.S., "Mathematical Models of Human Pilot Behavior," AGARD-AG-188, Jan. 1974.

[5]Hess, R.A., "A Dual-Loop Model of the Human Controller," *Journal of Guidance and Control,* Vol. 1, July-Aug. 1978, pp. 254-260.

[6]Hess, R.A., "A Rationale for Human Operator Pulsive Control Behavior," *Journal of Guidance and Control,* Vol. 2, May-June 1979, pp. 221-227.

[7]Hess, R.A., "A Structural Model of the Adaptive Human Pilot," *Journal of Guidance and Control,* Vol. 3, Sept.-Oct. 1980, pp. 416-423.

[8]Hess, R.A., "Pursuit Tracking and Higher Levels of Skill Development in the Human Pilot," *IEEE Transactions on Systems, Man, and Cybernetics,* Vol. SMC-11, April 1981, pp. 262-273.

[9]McRuer, D.T., "Human Dynamics in Man-Machine Systems," *Automatica,* Vol. 16, May 1980, pp. 237-253.

[10]Granit, R., *The Basis of Motor Control,* Academic Press, London and New York, 1970.

[11]McRuer, D.T. and Magdaleno, R.E., "Human Pilot Dynamics with Various Manipulators," AFFDL-TR-66-138, Dec. 1966.

[12]Gordon-Smith, M., "An Investigation into Some Aspects of the Human Operator Describing Function While Controlling a Single Degree of Freedom," *Proceedings of the Fifth Annual Conference on Manual Control,* March 1969, pp. 203-240.

[13]Hoh, R.H., Craig, S.J., and Ashkenas, I.L., "Identification of Minimum Acceptable Characteristics for Manual STOL Flight Path Control," Federal Aviation Administration, FAA-RD-75-123, June 1976.

[14]Hindson, W.S., Hardy, G.H., and Innis, R.C., "Flight Test Evaluation of STOL Control and Flight-Director Concepts in a Powered-Lift Aircraft Flying Curved Decelerating Approaches," NASA TP 1641, 1981.